

# Infrequent Triggering of Tremor along the San Jacinto Fault near Anza, California

by Tien-Huei Wang, Elizabeth S. Cochran, Duncan Agnew, and David D. Oglesby

**Abstract** We examine the conditions necessary to trigger tremor along the San Jacinto fault (SJF) near Anza, California, where previous studies suggest triggered tremor occurs, but observations are sparse. We investigate the stress required to trigger tremor using continuous broadband seismograms from 11 stations located near Anza, California. We examine 44  $M_w \geq 7.4$  teleseismic events between 2001 and 2011; these events occur at a wide range of back azimuths and hypocentral distances. In addition, we included one smaller-magnitude, regional event, the 2009  $M_w$  6.5 Gulf of California earthquake, because it induced extremely high strains at Anza. We find the only episode of triggered tremor occurred during the 3 November 2002  $M_w$  7.8 Denali earthquake. The tremor episode lasted 300 s, was composed of 12 tremor bursts, and was located along SJF at the northwestern edge of the Anza gap at approximately 13 km depth. The tremor episode started at the Love-wave arrival, when surface-wave particle motions are primarily in the transverse direction. We find that the Denali earthquake induced the second highest stress ( $\sim 35$  kPa) among the 44 teleseismic events and 1 regional event. The dominant period of the Denali surface wave was 22.8 s, at the lower end of the range observed for all events (20–40 s), similar to periods shown to trigger tremor in other locations. The surface waves from the 2009  $M_w$  6.5 Gulf of California earthquake had the highest observed strain, yet a much shorter dominant period of 10 s and did not trigger tremor. This result suggests that not only the amplitude of the induced strain, but also the period of the incoming surface wave, may control triggering of tremors near Anza. In addition, we find that the transient-shear stress (17–35 kPa) required to trigger tremor along the SJF at Anza is distinctly higher than what has been reported for the well-studied San Andreas fault.

## Introduction

Tectonic tremor, also known as nonvolcanic tremor (NVT), has been widely observed around the world, in both subduction zones and crustal regions close to well-developed strike-slip faults (e.g., Obara, 2002; Rogers and Dragert, 2003; Obara *et al.*, 2004; Nadeau and Dolenc, 2005; Shelly *et al.*, 2006; Schwartz and Rokosky, 2007). Tremor has been observed to occur spontaneously (e.g., Obara, 2002; Rogers and Dragert, 2003; Obara *et al.*, 2004; Nadeau and Dolenc, 2005; Shelly and Hardebeck, 2010), but their occurrence can also be modulated by tidal forces (e.g., Rubinstein *et al.*, 2008; Thomas *et al.*, 2009) and teleseismic surface-wave arrivals (e.g., Miyazawa and Mori, 2005, 2006; Rubinstein *et al.*, 2007; Gomberg *et al.*, 2008; Miyazawa and Brodsky, 2008; Peng and Chao, 2008; Peng *et al.*, 2008; Rubinstein *et al.*, 2009; Gonzalez-Huizar *et al.*, 2012). Tremor episodes triggered by the dynamic stress changes imposed by passing surface waves are well correlated with surface-wave peak amplitudes (e.g., Gomberg *et al.*, 2008; Peng *et al.*, 2008). Triggered tremor has been shown to be modulated by either

teleseismic Love- or Rayleigh-wave arrivals, depending on the tectonic regime and fault plane orientation (Hill, 2012b). These observations of remote triggering hold clues to the failure-stress conditions on the deep fault (below typical seismogenic depths), and perhaps imply different material properties, such as high fluid pressures and/or lower effective friction at or near the location of the triggered tremor. Specific failure conditions, including the amplitude and type of triggering stress, can illuminate the conditions necessary to generate tremor.

Remote triggering of tremor is widely documented in various tectonic regions as the number of tremor observations has accumulated in recent years. However, the type of surface waves shown to trigger tremor appears to vary by region and/or faulting type. In subduction zones, studies in Japan report that tremor is modulated by the Rayleigh-wave arrival (Miyazawa and Mori, 2005, 2006; Miyazawa and Brodsky, 2008), whereas in Cascadia (Rubinstein *et al.*, 2007) and Taiwan (Peng and Chao, 2008) tremor is shown

to start at the Love-wave arrival. Miyazawa and Mori (2005, 2006) and Miyazawa and Brodsky (2008) suggest that volumetric strain changes due to the Rayleigh-wave arrival play a strong role in triggering tremor observed in Japan. The volumetric strain may cause dilatation on the fault, reducing friction, which acts to trigger tremor (Rubinstein *et al.*, 2007). Miyazawa and Brodsky (2008) propose that the presence of fluid-induced volumetric strain modulates the normal stress, causing strong triggering. According to Hill (2012b), Rayleigh waves encourage failure on normal faults above  $\sim 13$  km depth and encourage failure on thrust faults at deeper depths, where incoming waves are normal to fault strike. In contrast, Love waves induce large differential stresses across the fault surface with peak strains occurring when incident surface waves are parallel to fault strike (Hill, 2012b). Rubinstein *et al.* (2007) showed that shear-stress changes induced by passing Love waves due to the 2002  $M$  7.8 Denali earthquake triggered tremor in Cascadia. They noted that incident Love waves were parallel to the trench and, thus, encouraged tremor occurrence. Peng and Chao (2008) also concluded that tremor on a detachment fault underneath the Central Range in Taiwan was likely triggered by the Love-wave arrival. They suggested that triggering was coincident with the Love and not the Rayleigh wave due to the higher amplitude of the Love wave, estimated to be roughly four times larger than the Rayleigh wave.

Along strike-slip faults in California, Gombert *et al.* (2008) reported the 2002 Denali  $M_w$  7.8 earthquake triggered tremor in multiple locations, including along the San Andreas fault (SAF) and on the San Jacinto fault (SJF) near Anza in southern California. Peng *et al.* (2008) suggest tremor observed along the SAF near Cholame was triggered by the Love-wave arrival. They showed that peaks in the envelope of the tremor signal correlated with the Love-wave peak amplitude, after applying source-station travel-time corrections. Both Peng *et al.* (2008) and Hill (2012b) noted that Love waves preferentially trigger tremor on vertical strike-slip faults when the incident wave is approximately parallel or normal to fault strike. Several recent studies have shown that tremor is routinely triggered on the Parkfield–Cholame section of the SAF by both teleseismic and regional surface-wave arrivals (Peng *et al.*, 2008; Shelly *et al.*, 2009). Along the SAF, tremor occurs at depths between 15–40 km depth, with the most abundant tremor occurring near the along-strike transition between the locked and creeping section under Cholame, California (Nadeau and Dolenc, 2005; Peng *et al.*, 2009; Shelly *et al.*, 2009). It is worth noting that physical conditions along crustal faults in California are likely to differ significantly from subduction-zone settings. In particular, tremor in subduction zones have been inferred to occur in regions of high pore pressures (Brown *et al.*, 2005; Shelly *et al.*, 2006), yet there is no obvious source of fluid along the southern SAF or the SJF at the depths where tremor has been observed. Thus, it is important to examine the conditions needed to trigger tremor along crustal faults such as the SJF.

Here, we report our observations of triggered tremor along the SJF near Anza, California. The Anza region of the SJF is an ideal location for such study as triggered tremor has previously been reported (Gombert *et al.*, 2008; Chao, Peng, Fabian, *et al.*, 2012). A seismic network of surface and borehole stations provides a dense set of seismic observations necessary to identify tremor. Additionally, the long-base strainmeters at Piñon Flat Observatory (PFO) measure surface strains directly. Using the data from 44 teleseismic events, we examine whether the amplitude, frequency content, and/or orientation of the triggering surface wave controls triggering of tremor. We determine the shear stress induced by each event using the estimated strain primarily based on seismic-velocity records. The measured surface strain at PFO is then used to verify consistency and correctness of the estimated strain. In addition, we estimate the location of the triggered tremor and report its frequency and amplitude characteristics. The results are compared to triggered tremor observed previously in a variety of tectonic settings.

### San Jacinto Fault Background

In southern California, the majority of the strain across the plate boundary is not solely accommodated on the SAF; instead, it is distributed across the SAF, San Jacinto (SJF), and Elsinore faults. The surface expression of the SJF is composed of a series of widely spaced, en echelon strands with relatively complex geometry. In addition, the SJF appears to consist of several distinct fault segments according to interpretations of slip rate, historical earthquakes, background seismicity, and state of stress. From paleoseismic studies, the slip rate of SJF generally decreases from 20 mm/yr along the northwestern segment (Kendrick *et al.*, 2002), to 12–14 mm/yr along its central segment at Anza, (Rockwell *et al.*, 1990), to 8–15 mm/yr along the southeastern segment (Sharp, 1967; Fig. 1).

Historically, the SJF has been the most seismically active fault in southern California, with a high rate of moderate to large earthquakes in the past 100–150 yr (Thatcher *et al.*, 1975; Sanders and Kanamori, 1984; Sanders and Magistrale, 1997). However, a 20–50 km segment near the central portion of the SJF, known as the Anza seismic gap (Sanders and Kanamori, 1984; see Fig. 2), has not had a large surface-rupturing earthquake ( $M_L \geq 6.5$ ) since 1899 (Thatcher *et al.*, 1975; Rockwell *et al.*, 1990). The Anza gap is bounded to the northwest by a segment that ruptured in the 1918  $M_L$  6.8 earthquake and to the southeast by the Borrego Mountain segment that ruptured in the 1968  $M_w$  6.5 earthquake (Thatcher *et al.*, 1975; Heaton and Helmsberger, 1977; Sanders and Kanamori, 1984; Steidl *et al.*, 2000). Sanders and Kanamori (1984) suggested the Anza gap segment was likely to rupture in a moderate to large earthquake because the segment had not ruptured in historic time (Thatcher *et al.*, 1975; Sykes and Nishenko, 1984). With a strain accumulation of approximately 8–12 mm/yr, Rockwell *et al.* (1990) estimated at least 0.8 m has accumulated on the segment. The

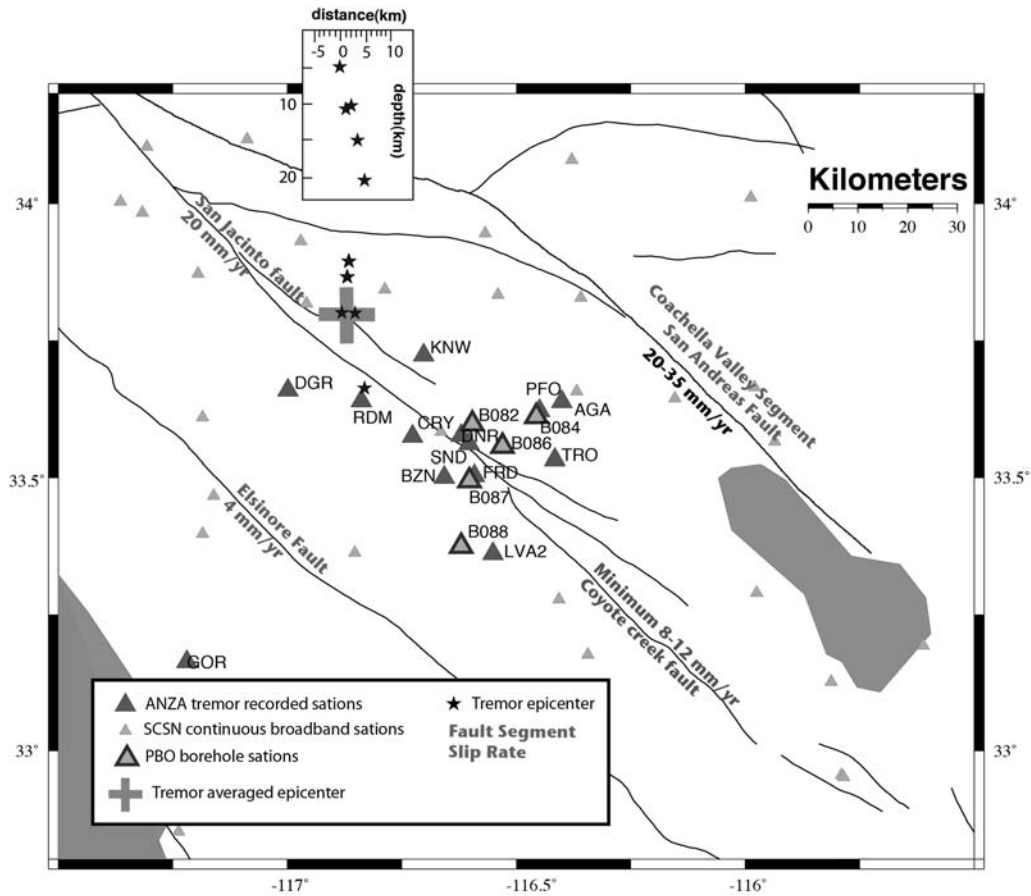


**Figure 1.** Map showing all Southern California Seismic Network (SCSN) continuous broadband stations (small light gray triangles), stations that observe tremor (dark gray triangles), and borehole seismic stations (gray triangles with a black border). The black stars indicate the estimated location of each tremor low-frequency earthquake (LFE). The upper left, small rectangular inset shows the depth profile of the estimated hypocenters for each of the five tremor LFEs. The vertical and horizontal scales on both profiles are in kilometers. The slip rates for each of the major faults are shown. Slip rate references: Coachella Valley (Sanders, 1990), SJF (Sanders and Kanamori, 1984), southern SJF (Sanders and Kanamori, 1984), and Elsinore (Sieh, 1986).

size of the future Anza seismic-gap earthquake was estimated to be  $M$  6.5 along a fault segment 20 km long and 15 km deep (Sanders and Kanamori, 1984; Rockwell *et al.*, 1990). It was suggested that the high rate of small earthquakes since 1970 at the edge of this gap indicated that the fault was critically stressed and likely to fail (Sanders and Kanamori, 1984). Although no evidence has since been found at the surface suggesting strain is being accommodated by aseismic creep (Louie *et al.*, 1985; Vanboskirk *et al.*, 2011), Wdowinski (2009) inferred deep creep was occurring based on seismic and geodetic observations.

The pattern of earthquakes along the SJF suggests distinct changes occur along fault strike, both from the seismicity rate and in the depth extent of the seismogenic zone. In Figure 2, we plot seismicity above  $M_L$  2.0 from 1996–2005 (Fig. 2). The depth of the seismogenic zone varies from about 11–12 km depth to the north to as deep as 20 km near the central section of the fault. Sanders and Magistrale (1997) reported an abrupt change in the maximum hypocentral depth of earthquakes about midway along the SJF. This abrupt change in hypocentral depth coincides with a change in the pattern of

seismicity from very well-aligned, deep earthquakes to the south to diffuse, shallower seismicity to the north.

Several studies also suggest that the state of stress along the SJF may be quite heterogeneous. Hartse *et al.* (1994) analyzed focal mechanisms and found notable stress anomalies within the Anza seismic gap. They reported a significant change in orientation of focal mechanisms (maximum compressive stress  $74^\circ \pm 13^\circ$  relative to fault strike, compared to  $62^\circ \pm 11^\circ$  northwest and  $49^\circ \pm 7^\circ$  southeast) and suggested that this may result from stronger material within the gap. More recently, Bailey *et al.* (2010) suggested that stress heterogeneity may be controlled by the complex-fault structures. They observed two clusters of earthquakes with primarily thrust mechanisms to the northwest and strike-slip mechanisms to the southeast of the Anza gap (Bailey *et al.*, 2010).

## Data and Methods

We examine continuous seismograms recorded along the SJF near Anza, California, for triggered tremor and data from 11 surface stations, 8 of them from the Anza network,

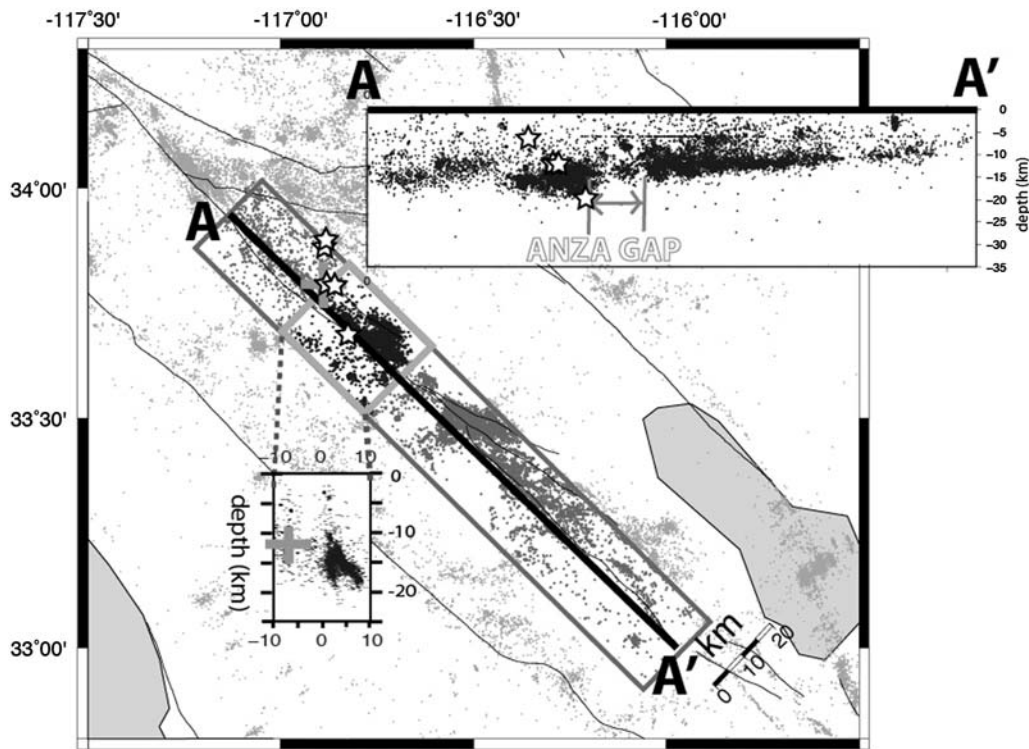


**Figure 2.** Seismicity map along the SJF. Seismicity (small circles) from 1996–2005 is shown as reported in the SCEC catalog. Stars indicate the estimated locations of the LFE templates. Light gray cross indicates the average location of tremor. The upper right cross section is a vertical profile of seismicity along A–A', a simplified surface fault trace for the SJF fault plane (N43°W, vertical dip). This profile includes seismicity within 10 km of each side of A–A' (dark gray rectangular box). The depth profile at the lower left corner shows seismicity particularly near the northwestern edge of the Anza gap, as indicated by the light gray box. Note that the white stars are hypocenters of tremor templates and the gray cross is the average location of tremors, which correspond to the locations in Figure 1.

and 3 from Southern California Seismic Network (SCSN). We also included five Plate Boundary Observatory (PBO) borehole stations (Fig. 1). Borehole-station installations were completed in 2006 and are used when available. We examined 44 large teleseismic earthquakes ( $M_w \geq 7.4$ ) that occurred between 2001 and 2011 at epicentral distances greater than 2000 km from Anza; this distance was chosen such that surface waves are clearly separated from the body-wave arrivals. The events occur at a range of back azimuths, from 128° to 352° (see Table 1). Figure 3 shows the locations of the 44 events relative to the Anza array. We also utilize data from 17 small local earthquakes that occurred in 2002 ( $M_L$  1.2–1.47; Table 2) to compare frequency spectra between tremor, noise, and local earthquakes (Fig. 4).

#### Tremor Identification and Template Method

To identify tremor, we visually examined a window around the teleseismic arrivals, from the onset of the  $P$ -wave arrival until amplitudes return to background noise levels. We band-pass filtered the data between 2–6 Hz and visually inspected the three components for tremor. By visual inspection, we found only one episode of triggered tremor that occurred during the 3 November 2002  $M_w$  7.8 Denali earthquake. As previous studies have indicated (e.g., Aguiar *et al.*, 2009; Brown, 2010; Chao, Peng, Fabian, *et al.*, 2012), trig-

gered tremor might be obscured by background noise. To ensure that even low-amplitude tremor episodes were detected, we also manually selected LFE (low-frequency earthquake) templates from the tremor episode identified during the Denali earthquake. Here, we adopted the template matching method of Shelly *et al.* (2006). The template method assumes repeated LFEs occur close to or at the same location, therefore generating waveforms with high similarity. We selected 6 s windows around times of higher amplitude tremor (e.g., LFEs) on 11 stations that recorded the tremor at high signal-to-noise ratios (Fig. 5). We centered the 6 s window on the maximum amplitude of the envelope function, assuming the high amplitude burst was coincident with the tremor  $S$ -wave arrival. To define a template, the same time window was chosen for the two horizontal components on a given station. Using this method, we initially selected five templates from the Denali tremor episode. As shown in Figure 4, we verified the templates were tremor by comparing the frequency spectra of the tremor to background noise and a set of 17 local earthquakes ( $M_L$  1.2–1.47; Table 2). We then cross correlated the template LFEs across the 44 time series at the station sample rate to search for repeated LFEs. We cross correlate the templates across a window that started 1 h before the teleseismic  $P$ -wave arrival and ended 1 h after the main teleseismic energy has passed. Following the

**Table 1**  
Information about forty four large teleseismic events

Number	Date/Time (yyyy/mm/dd hh:mm:ss.s)	Latitude	Longitude	Azimuth (°)	Distance (km)	$M_w$	Depth (km)	Dominant Period (T)	Observed FP Strain	Observed FN Strain	Estimated FP Strain	Estimated FN Strain	FP Velocity (Normalized)	FN Velocity (Normalized)	FN Stress (kPa)	FP Stress (kPa)
1	2001/01/26 03:16:54.9	23.6	70.2	352	13603	7.6	19.8	34	X	X	32	27	0.04	0.02	1.43	1.72
2	2001/06/23 20:34:23.3	-17.3	-72.7	133	7344	8.4	29.6	59	159	255	162	231	0.19	0.18	12.46	8.81
3	2001/07/07 9:39:1.8	-17.5	-72.5	133	7376	7.6	25.0	59	X	X	19	15	0.02	0.01	0.81	1.02
4	2001/11/14 9:27:15.9	35.8	92.9	335	11698	7.8	15.0	43	X	X	46	54	0.05	0.04	2.93	2.50
5	2002/03/05 21:16:23.3	5.9	124.3	292	12240	7.5	28.7	56	X	X	11	4	0.01	0.00	0.22	0.61
6	2002/09/08 18:44:38.3	-3.3	143.4	273	11114	7.6	19.5	33	X	X	26	26	0.03	0.02	1.40	1.43
7	2002/10/10 10:50:41.9	-1.8	134.3	279	11858	7.5	15.0	68	X	X	20	28	0.02	0.02	1.50	1.07
8	2002/11/03 22:13:28.0	63.2	-144.9	338	3820	7.8	15.0	23	X	X	870	1,315	2.00	1.00	71.04	47.43
9	2003/01/22 02:06:48.9	18.9	-103.9	139	2085	7.5	26.0	24	X	X	106	156	0.12	0.12	8.40	5.79
10	2003/07/15 20:28:37.6	-1.4	69.5	348	16373	7.5	15.0	59	X	X	14	19	0.02	0.01	1.04	0.76
11	2003/08/04 4:37:42.5	-60.8	-43.2	150	12416	7.6	15.0	69	X	X	15	17	0.02	0.01	0.92	0.80
12	2003/09/25 19:50:38.2	42.2	143.8	311	8251	8.3	28.2	66	X	X	121	66	0.14	0.05	3.59	6.61
13	2003/11/17 6:43:31.0	51.1	177.9	311	5503	7.7	21.7	48	X	X	22	17	0.03	0.01	0.89	1.19
14	2004/11/11 21:26:58.0	-7.9	125.1	279	13078	7.5	17.0	41	8	5	6	8	0.01	0.01	0.41	0.33
15	2004/12/23 14:59:30.9	-49.9	161.3	223	12275	8.1	27.5	80	X	X	121	24	0.14	0.02	1.29	6.61
16	2004/12/26 1:19:0	3.1	94.3	315	14789	9.0	28.6	55	X	X	264	171	0.30	0.13	9.23	14.40
17	2005/03/28 16:10:31.5	1.7	97.1	311	14724	8.6	25.8	37	61	78	57	67	0.06	0.05	3.63	3.08
18	2005/10/08 3:50:51.5	34.4	73.5	351	12376	7.6	12.0	45	20	28	26	26	0.03	0.02	1.38	1.44
19	2006/04/20 23:25:17.6	60.9	167.1	325	6056	7.6	12.0	50	46	46	41	64	0.05	0.05	0.65	0.47
20	2006/07/17 8:20:38.4	-10.3	107.8	289	14789	7.7	20.0	37	4	3	7	5	0.01	0.00	0.29	0.36
21	2006/11/15 11:15:8.0	46.7	154.3	311	7282	8.3	13.5	99	60	55	50	71	0.06	0.05	3.81	2.74
22	2007/01/13 4:23:48.1	46.2	154.8	310	7273	8.1	12.0	37	114	124	92	108	0.11	0.08	5.82	5.02
23	2007/01/21 11:28:1.0	1.1	126.2	287	12399	7.5	22.2	59	5	9	8	12	0.01	0.01	0.62	0.46
24	2007/04/01 20:40:38.9	-7.8	156.3	262	10195	8.1	14.1	41	X	X	33	29	0.04	0.02	1.57	1.79
25	2007/08/15 23:41:57.9	-13.7	-77.0	135	6746	8.0	33.8	52	63	72	75	47	0.09	0.04	2.52	4.07
26	2007/09/12 11:11:15.6	-3.8	101.0	302	14883	8.5	24.4	31	20	22	37	48	0.04	0.04	2.62	2.01
27	2007/09/30 5:23:51.5	-49.3	164.0	223	12066	7.4	12.6	19	9	7	12	7	0.01	0.01	0.39	0.68
28	2007/11/14 15:41:11.2	-22.6	-70.6	135	7943	7.7	37.6	85	14	24	22	17	0.03	0.01	0.90	1.20
29	2008/05/12 6:28:40.4	31.4	104.1	325	11602	7.9	12.8	48	48	31	47	60	0.05	0.05	3.24	2.56
30	2009/01/03 19:44:9.0	-0.6	132.5	281	11946	7.4	18.2	80	17	10	24	20	0.03	0.02	1.07	1.33
31	2009/07/15 9:22:49.6	-45.9	166.3	225	11723	7.8	23.5	59	24	16	29	18	0.03	0.01	1.00	1.60
32	2009/08/03 18:00:06.5	29.2	-113.5	146	583	6.9	12.2	10	1497	1937	1,002	2,342	1.15	1.78	126.45	54.60
33	2009/08/10 19:56:5.0	14.2	92.9	324	13834	7.5	22.0	51	9	9	9	10	0.01	0.01	0.53	0.48
34	2009/09/29 17:48:26.8	-15.1	-172.0	237	7967	8.1	12.0	51	65	108	78	153	0.09	0.12	8.27	4.23
35	2010/02/27 6:35:14.5	-36.0	-73.2	145	8973	8.8	23.2	100	246	278	268	322	0.31	0.22	15.55	13.47
36	2010/02/27 8:1:29.8	-38.1	-75.4	148	9051	7.4	19.9	77	X	X	23	46	0.03	0.03	2.48	1.28
37	2010/04/06 22:15:19.1	2.1	96.7	312	14712	7.8	17.6	24	13	17	20	12	0.02	0.01	0.64	1.07
38	2010/06/12 19:27:0.4	7.9	91.7	322	14509	7.5	33.1	65	16	11	12	24	0.01	0.02	1.32	0.64
39	2010/10/25 14:42:59.8	-3.7	99.3	304	15007	7.8	12.0	24	4	5	5	5	0.01	0.00	0.29	0.25
40	2010/12/21 17:19:53.6	27.1	143.8	298	9169	7.4	15.6	46	13	14	16	15	0.02	0.01	0.82	0.88

(continued)

**Table 1 (Continued)**

Number	Date/Time (yyyy/mm/dd hh:mm:ss.s)	Latitude	Longitude	Azimuth (°)	Distance (km)	$M_w$	Depth (km)	Dominant Period (T)	Observed FP Strain	Observed FN Strain	Estimated FP Strain	Estimated FN Strain	FP Velocity (Normalized)	FN Velocity (Normalized)	FN Stress (kPa)	FP Stress (kPa)
41	2011/03/11 5:47:32.8	37.5	143.1	307	8585	9.1	20.0	103	223	286	257	296	0.30	0.23	16.01	14.02
42	2011/07/06 19:33:2.5	-29.2	-175.8	229	9345	7.6	22.3	69	12	22	16	26	0.02	0.02	1.39	0.89
43	2011/10/21 17:57:28.3	-29.0	-176.2	229	9360	7.4	33.0	46	8	22	21	15	0.02	0.01	0.79	1.15

The events in bold texts are the events which induced (1) Second highest amplitude of shear stress, by 2002 Denali earthquake; event (Number 8), and (2) the highest shear strain and stress, by 2009  $M_w$  6.9 Gulf of California earthquake; event (Number 32). The back azimuths are measured from station RDM. An X in the observed fault-parallel (FP) and fault-normal (FN) strain columns indicates that surface strain measurements are not available or not complete for the event. One regional event, the 2009  $M_w$  6.9 Gulf of California earthquake (Number 32), is included due to the large strain it induced at Anza.

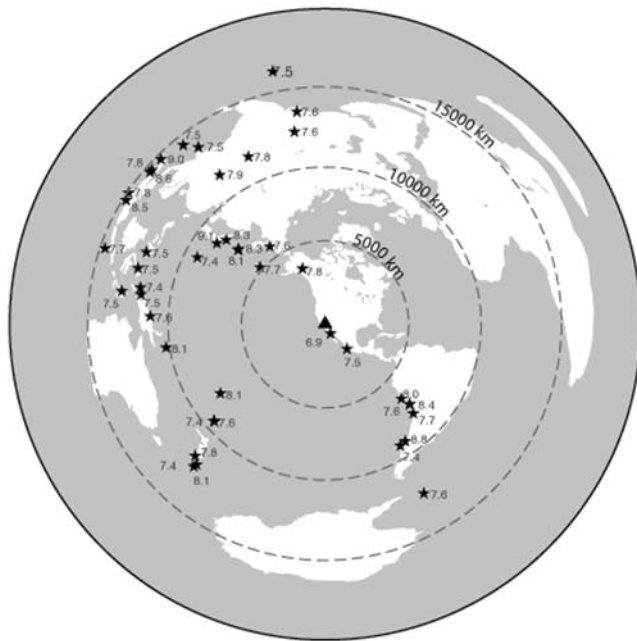


**Figure 3.** Global map of 44 teleseismic earthquakes examined. Black stars are teleseismic earthquake epicenters with magnitudes ( $M_w$ ) indicated. The triangle in the center of this map represents the approximate location of the seismic stations near Anza. The gray dashed circles mark equal distance contour to Anza every 5000 km.

method of Shelly *et al.* (2006), we fixed the moveout across the array for each LFE template during cross correlation (cc). This fixed moveout limits detection to signals highly similar to the template LFE, requiring similar hypocenter location and source mechanism.

To determine when a repeat of the template event occurs, we first summed the correlation values across the horizontal

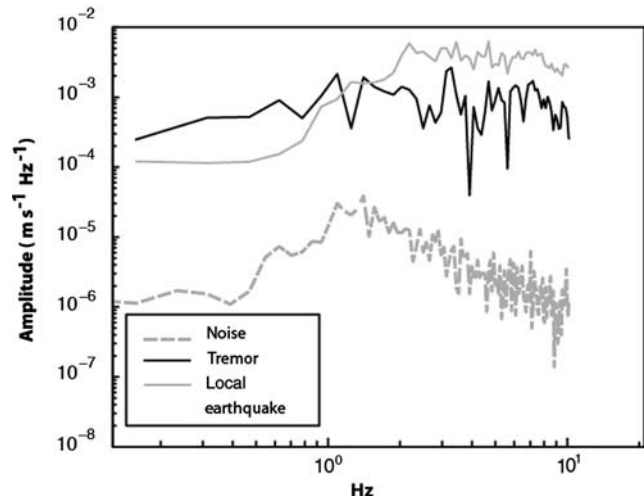


**Figure 4.** Frequency spectra of a small earthquake, tremor and noise are plotted together for comparison. These curves are taken from station RDM, north component. The spectrum of small earthquakes is averaged from displacement record of 17 local earthquakes selected in the Anza region (Table 2). The noise curve is averaged from 17 time windows before each  $P$  picks of local earthquakes. These spectra are generated from displacement records of similar time duration. Note that tremor is lacking in frequency above 6 Hz compared to the earthquake spectra. However, tremor abounds in low frequency energy below 6 Hz relative to noise. Note that record above 10 Hz (Nyquist frequency) may have artificial effect, which is not valid.

components of 11 stations (22 components in total) and then determined if that summed correlation value exceeded an assigned threshold. The threshold is set to 4.0, corresponding to a correlation value of 0.18 or higher per trace, on average. Figure 6a shows the times when the correlation value

**Table 2**  
Sixteen Local Earthquakes with Hypocenters Close to the Estimated Tremor Locations and Similar Velocity Amplitude on  $S$  Arrivals

Date/Time (yyyy/mm/dd hh:mm:ss.s)	Magnitude $M_L$	Latitude	Longitude	Depth (km)
2002/01/21 17:37:23.21	1.29	33.645	-116.786	17.4
2002/02/11 5:55:15	1.21	33.984	-116.607	12.4
2002/03/02 14:41:44.82	1.21	33.713	-116.825	15
2002/04/02 15:27:21.52	1.22	33.695	-116.763	15.9
2002/05/17 3:15:0.25	1.47	33.696	-116.719	18.4
2002/05/18 7:28:9.56	1.29	33.661	-116.721	17.4
2002/05/19 15:8:9.81	1.27	33.724	-116.755	18.6
2002/06/29 13:35:3.59	1.22	33.974	-116.744	17.1
2002/07/02 11:38:18.93	1.21	33.688	-116.719	17.4
2002/08/04 22:40:7.8	1.21	33.712	-116.819	15.3
2002/08/16 2:15:41.95	1.21	33.682	-116.777	15.2
2002/09/18 0:38:40.86	1.45	33.871	-116.803	15.2
2002/10/10 10:42:21.04	1.28	33.73	-116.776	18.4
2002/11/02 3:13:17.44	1.2	33.723	-116.775	17.8
2002/11/19 11:55:10.85	1.42	33.684	-116.75	18
2002/12/12 2:44:29.17	1.2	33.678	-116.672	17.1

These local events are selected based on magnitude and hypocentral locations. We select these small earthquakes with velocity amplitude similar to the tremor pulses found in this study. We select the local small earthquakes with hypocenters close to the approximated tremor source.

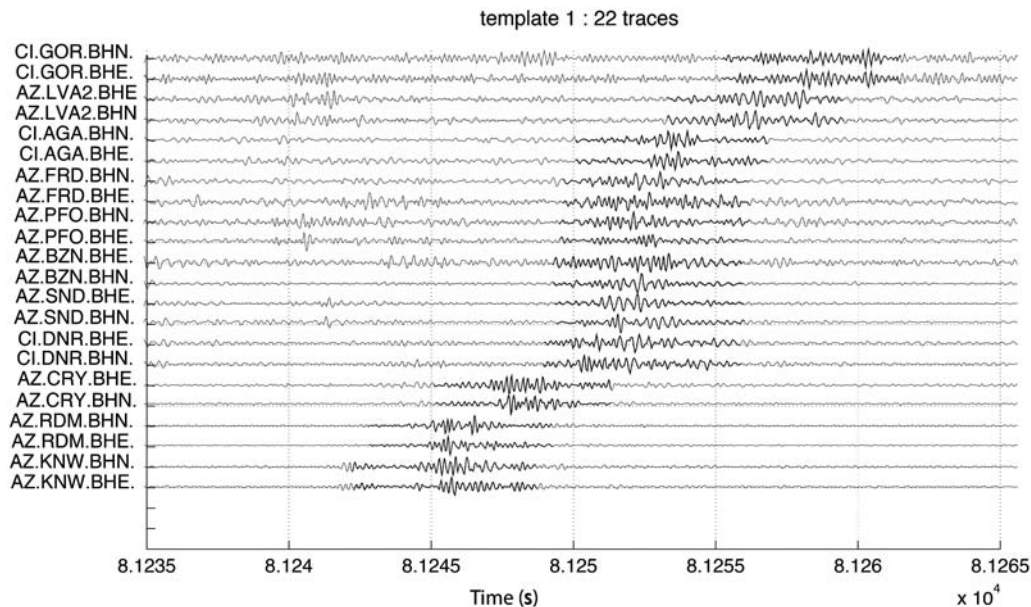


**Figure 5.** A handpicked tremor template during the Denali earthquake surface wave shown in descending order of arrival times. The bold portion of each trace is the 6 s template window for each component (horizontal) and station. We picked the template to span the maximum amplitude of the envelope function, which is assumed to be the  $S$  arrival of each LFE. The time of this LFE template relative to other LFEs in the tremor episode is shown in Figure 6a (gray portion). This template is used to search for repeating LFEs within the continuous time series of the 44 teleseismic events.

exceeded the defined threshold for a particular template during the Denali teleseismic arrivals. We used this threshold to search for repeated LFEs during all 44 teleseismic earthquakes. It is worth noting that the template method applied here can only detect LFEs that repeat with similar source characteristics at similar locations; an LFE that occurs at a different location from the template LFEs will not be identified.

#### Source Location

To estimate the location of tremor observed during the Denali earthquake, we manually picked the maximum amplitude of the LFE, assumed to be the  $S$ -wave arrival, on each of the 11 stations.  $S$ -wave arrivals were picked on each of the five template events. The source location of the tremor is not precisely known because lower amplitude  $P$ -wave arrivals were not visible and  $S$ -wave picks were poorly constrained due to their emergent nature on the tremor records. Stacking the tremor templates did not significantly improve the visibility of the phase arrivals, so we instead chose to locate each of the templates independently to better estimate location errors. We used the generalized-earthquake-location (GENLOC; Pavlis *et al.*, 2004) package in Antelope to locate the LFEs. We adopted the velocity structure from the Southern California Earthquake Center Community Velocity Model (SCEC CVM-H 6.2; Suess and Shaw, 2003; Plesch *et al.*, 2011). The velocity model contains 14 layers with 2 km depth intervals and a lateral extent of 20 km across the SJF fault plane, as defined by SCEC Community Fault Model (SCECFM; Plesch *et al.*, 2007). Average error estimates from Antelope are approximately 0.1 km horizontally and 1 km in

depth, but these do not reflect the true errors due to the emergent nature of the arrivals. More accurate estimates of the error in tremor locations are determined by simply examining the range of locations determined for the five LFE templates (Fig. 1). As the templates all correlate highly with each other, we can reasonably assume they came from a small source region. The average hypocentral location for the five events is (33.87–116.98) with a standard deviation in horizontal location of 7.5 km. The depths of the tremor were poorly constrained due to a lack of  $P$ -wave arrivals and vary between 5 and 21 km depth.

#### Surface-Wave Stress and Strain Estimates

For each of the 44 teleseismic earthquakes, we measured the peak velocity amplitude of the surface wave first in the radial and transverse directions, to correlate tremor to the Rayleigh- and Love-wave arrivals. We then rotated the horizontal component seismogram to 317 (SJF fault strike) and 43 (fault normal). In doing so, the peak shear stress, contributed primarily by the Love wave (Hill, 2012a,b), is resolved into the fault-parallel and fault-normal directions. To estimate the peak amplitude in the tremor region, we use peak amplitude measurements on station RDM as it is both close to the estimated tremor epicenters and has a high signal-to-noise ratio. Following the work of Mikumo and Aki (1964), Gomberg and Agnew (1996), and Gomberg and Johnson (2005), we can derive the strain by partial derivative of the displacement

$$\varepsilon = \frac{\delta u}{\delta x} = \frac{\delta u}{\delta t} \frac{\delta t}{\delta x} = \frac{\delta u}{\delta t} \frac{1}{C}, \quad (1)$$

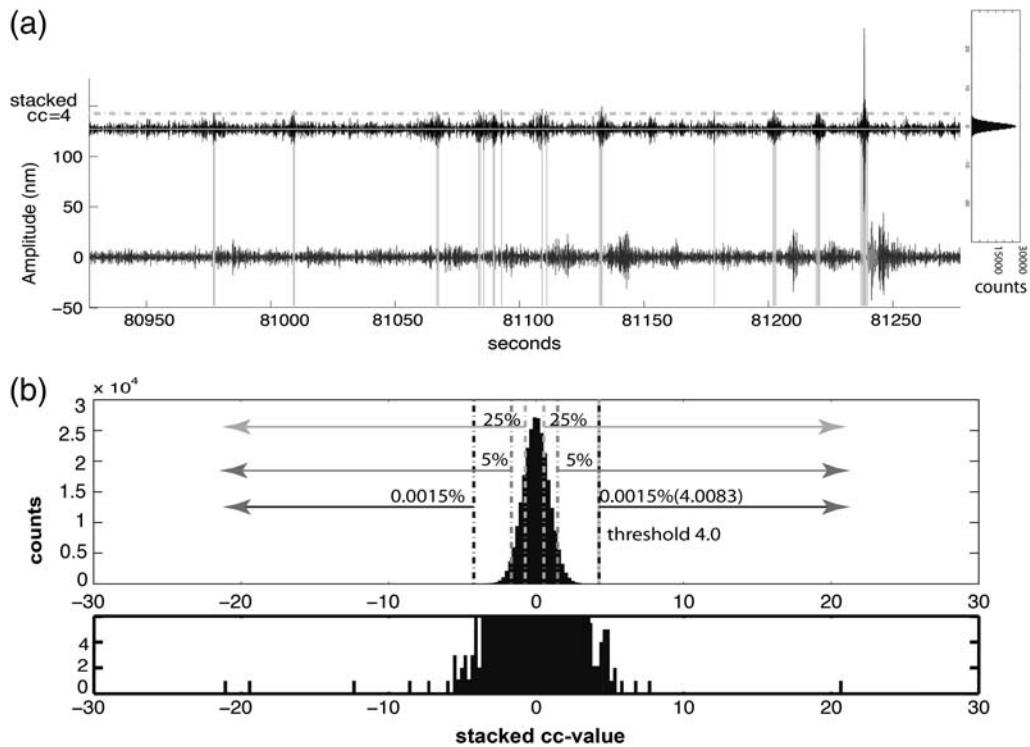


**Figure 6.** (a) Results after cross correlating a template LFE (Fig. 4) across the filtered Denali time series. Lower trace shows the filtered time series from station KNW, component BHE. The light gray trace at time 81,240 s corresponds to the time of template picked on this trace. Upper trace is the stacked cross-correlation values (cc values) versus time. The stacked cc values result from cross correlating the template with a fixed relative moveout on each trace and summed over 22 components. Gray vertical lines indicate the time when cross correlation is above the threshold cc value of 4.0 (horizontal gray dashed line), which we declare a detection. Note that the stacked cc value is 22 when LFE template exactly matches the time series. The overall stacked cc value has a normal distribution (small box at the right to black trace; see Fig. 6b for details). (b) Histogram of stacked cc values divided into 200 bins. The histogram shows the cc values are normally distributed. The threshold cc value of 4.0 only occurs in 0.0015% of the window. The dashed lines indicate probability of occurrence for different thresholds. The lower panel has enlarged scale on the y-axis in order to show the limited number of very high cc values, which correlate to times near the tremor template.

in which  $\varepsilon$  is the strain in the direction of propagation or normal to it,  $u$  is displacement,  $\frac{\partial u}{\partial x}$  represents strain in the direction  $x$ ,  $\frac{\partial u}{\partial t}$  is the particle velocity observed on seismic velocity record, and  $\frac{\partial u}{\partial t} = C$  is the local phase velocity of the Rayleigh wave or Love wave. Note that the incoming surface wave is assumed to be a plane wave that propagates at one phase velocity,  $C$ , in the direction of propagation.

We use a phase velocity of 4.0 km/s, averaged from the observed phase velocities that range from 3.5–4.5 km/s. The phase velocities ( $C$ ) are determined from the moveout of phase arrivals at several stations. We compare the strain estimates from the velocity seismograms with the strains observed at surface strainmeter PFO when fault-normal and fault-parallel strain records are available (Table 1). The peak velocities obtained at station PFO and RDM are similar, with less than 0.1% deviation; the distance between these two stations is negligible compared to the source–receiver distances, at  $\sim 1/100$  of the distance between source and receiver (Fig. 7). The surface strains estimated from the seismic data are consistent with the measured surface strains with a linear regression fit of  $R^2 = 0.99$  (Fig. 7).

## Results

### Observed Tremor

In initial analysis of the 2002 Denali earthquake, we found the highest amplitude bursts were detected as repeats of the template event (Fig. 6a). In fact, all of the selected template events from the Denali earthquake were found to correlate highly with each other, suggesting a single, small-source region for the tremor. We also determined the statistical significance of the summed correlation threshold using the Denali event as an example. During the 3.5 h window around the Denali earthquake, we cross correlated a 6 s window at the sample rate (20 samples per second), resulting in over 25,000 correlation windows. The summed cc values were normally distributed and 99.98% of the windows fall outside of the defined threshold (4.0). In other words, 0.02% of the windows exceeded the summed threshold and were considered a repeated LFE. Extending the analysis to 44 teleseismic earthquakes and one high amplitude regional event confirmed only one episode of triggered tremor; only the 2002  $M_w$  7.8 Denali earthquake resulted in triggering of tremor. This tremor episode is composed

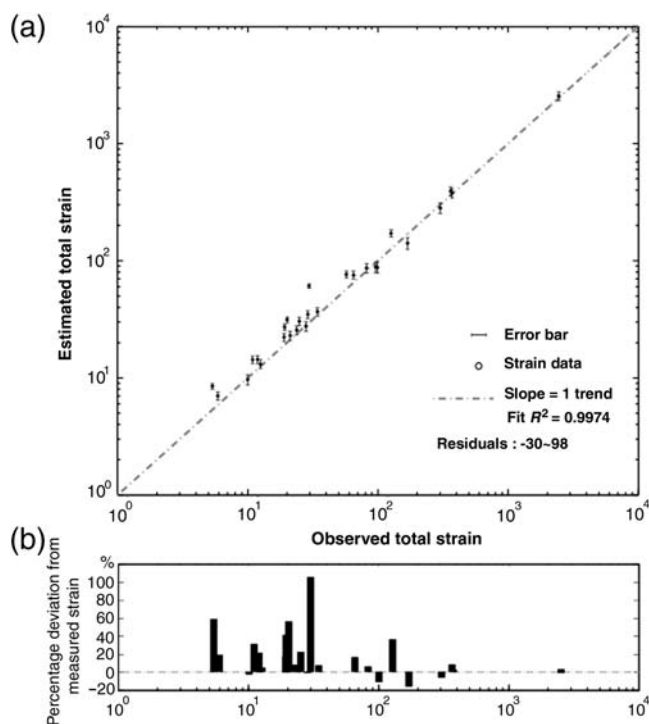


**Figure 7.** (a) Observed strain from strainmeter PFO and strain estimated from seismic velocity records on a log–log plot. The dashed gray line represents a slope of one. Error bars show the estimated uncertainty. The error bars on the y-axis represent an average of 18% uncertainty that results from the variation of phase velocity (3.5–4.5 km/s). The total strain is calculated as the vector sum of fault-normal and fault-parallel strains. The  $R^2$  value indicates how well the estimated total strains fits to a one-to-one relationship. (b) Residuals between the estimated strain and the one-to-one trend line. Note the percentage values are plotted on a linear-log scale to match the logarithm  $x$ -axis on the top plot (a).

of 12 LFE bursts in a 300 s period during the passage of the main surface-wave arrivals (Fig. 6a). The arrivals of these tremor bursts were slightly delayed compared to the peaks and troughs of the triggering wave. And, as shown in Figure 8, the amplitude of each tremor burst was not clearly modulated by the amplitude of the triggering surface wave.

### Triggering Factors: Amplitude and Period

We examined whether a given amplitude and/or period of surface wave was required to trigger tremor. We considered the peak strain amplitude measured on surface waves was representative of the peak stresses on the fault. Here, we assumed that when the peak stress exceeds a given threshold, tremor (e.g., slip) will occur on the fault. We report only the peak stress, as it is a simple metric to compare the teleseismic events. We found that the 2002 Denali earthquake had high strain amplitudes in both fault-parallel and fault-normal directions. In Figure 9, we show polar plots of the peak stress on fault-parallel and fault-normal directions, versus back azimuth for all 44 teleseismic events estimated from velocity records (see Table 1). Most of the events produced significantly lower strains than the Denali event; however, the 2009  $M_w$  6.9 Gulf of California earthquake produced strains approximately 1.5 times those of the Denali earthquake.

We also determined the dominant period of the surface waves for each of the 44 teleseismic events. The dominant period was estimated within a window that encompasses the initial arrivals of the Love and Rayleigh wave. The dominant period given in Table 1 is defined as the highest peak in the frequency spectrum within the time window around the surface wave. The uncertainty in the measured dominant period

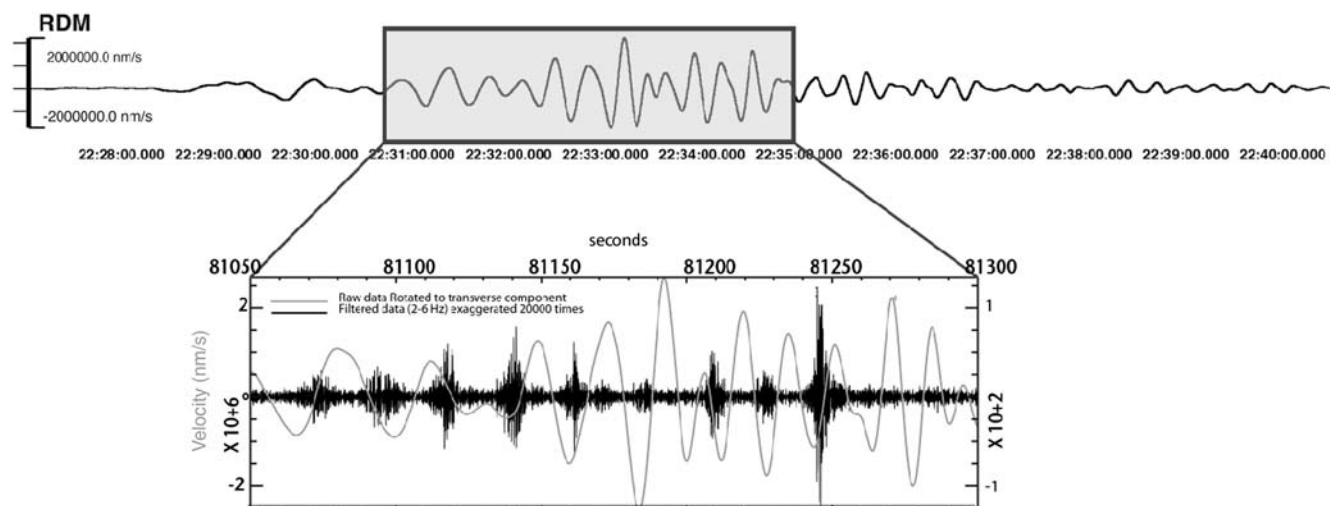


**Figure 8.** Upper trace shows an example waveform during surface wave of 2002  $M_w$  7.8 Denali earthquake showing the original surface-wave data (upper black trace) and the section enlarged below (shaded box). The lower trace shows the data filtered between 2–6 Hz (black trace) with clear tremor arrivals, and the original surface-wave data (gray trace). Traces shown here are recorded on the transverse component of station RDM.

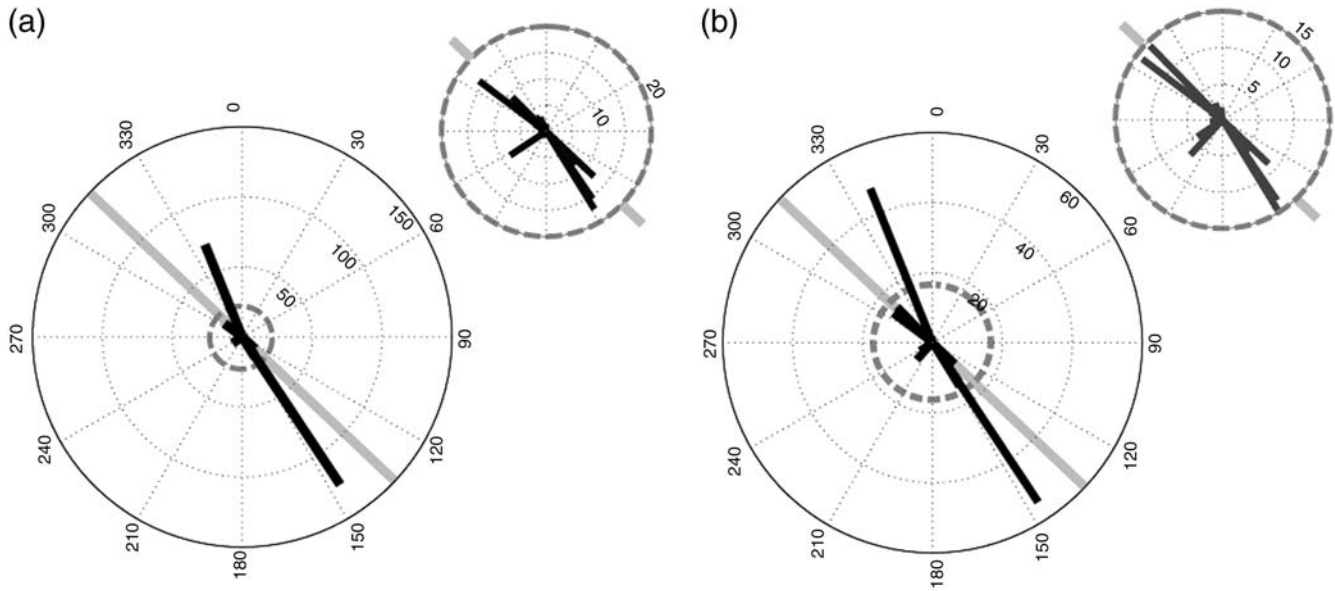


**Figure 9.** Polar plots of peak shear stress versus event back azimuth for the 44 teleseismic events. Such shear stresses are estimated from seismic-wave velocity in (a) fault-parallel and (b) fault-normal direction. Large polar plots show all 44 events scaled to the maximum observed shear stress. Smaller polar plots show the smaller strain values that are not visible on the full-scale plots. Note that the maximum radius of each circle is different, but the units are in kPa. The light gray lines indicate the strike of the SJF ( $317^\circ$ ).

shown in Figure 8 is defined as the range of periods with amplitudes equal to or greater than 60% of the peak amplitude. Windows encompassing just the Love or Rayleigh waves resulted in similar estimates of the dominant period as those determined for the combined window. Figure 10 shows the peak amplitude versus dominant period for all 44 teleseismic events. The dominant period of the 2002 Denali earthquake was 23 s, which was less than the mean period of the 44 teleseismic surface waves (54.5 s) but not the shortest period observed.

## Discussion

### Triggered Tremor Source

The triggered-tremor templates locate on, or very close to, the SJF, but the depth of the tremor was not well constrained. Within errors, we located the tremor to the northwestern end of the Anza gap, where there was a distinct change in the seismicity (Fig. 2; Thatcher *et al.*, 1975; Sanders and Kanamori, 1984). Gomberg *et al.* (2008) reported a similar estimate of the tremor location. Seismicity rates within the Anza gap are lower than adjacent sections of the fault (Sanders and Kanamori, 1984); although, the SJF has higher rates of moderate to large earthquakes compared to the other major strike-slip faults in the region, including the Elsinore and SAFs (Petersen and Wesnousky, 1994). In addition, along the Anza section of the SJF, the fault exhibits significant geometrical complexity, with multiple fault strands visible at depth in a cross section of the seismicity (Fig. 2).

There was also a step in source depths along strike of the SJF, with earthquakes in the Anza gap and farther south generally occurring shallower than 15 km and earthquakes

northwest of the gap occurring at depths up to 20–25 km (Fig. 2). Within the uncertainties in the estimated tremor-source depths it was difficult to constrain whether the tremor was occurring at the same depth or deeper than the background seismicity. Along the SAF near Parkfield, currently the only other strike-slip fault where tremor has been well-established based on data from a locally dense array, the tremor is estimated to occur below the main seismogenic zone between 15–40 km depths (Nadeau and Dolenc, 2005; Peng *et al.*, 2008, 2009), with more precise locations around

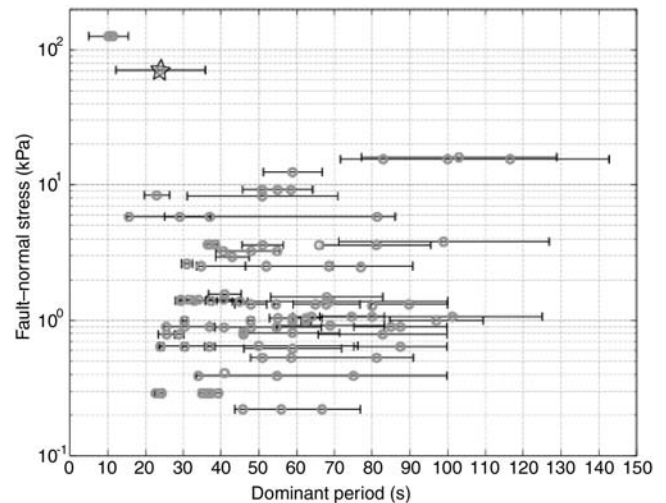


**Figure 10.** Peak shear stress versus dominant periods. Peak stress is estimated from observations at seismic station RDM. The error bars indicate uncertainties of dominant periods measured from the frequency spectra (see text in the section [Triggering Factors: Amplitude and Period](#)). The star highlights the 2002 Denali earthquake that triggered tremor.

25 km (Shelly *et al.*, 2009). Tremor observed both on strike-slip faults and along subduction zones are typically located below the main seismogenic zone, in the transition between the shallow, locked fault and deeper, creeping portions of the fault (Ito *et al.*, 2007; Schwartz and Rokosky, 2007).

#### Stress Amplitude Required for Triggering

The dynamic stress change induced by surface waves (e.g.,  $\sim 10$  kPa; Rubinstein *et al.*, 2008; Hill, 2012a) is typically a small fraction of the background lithospheric stress (1–100 MPa; Kanamori, 1980; Rubinstein *et al.*, 2010). However, studies have shown that earthquakes (e.g., Hill *et al.*, 1993; Gomberg *et al.*, 2003; Prejean *et al.*, 2004) and, more recently, tremor (e.g., Rubinstein *et al.*, 2007; Miyazawa *et al.*, 2008; Peng and Chao, 2008) can be triggered by passing teleseismic waves. The maximum-velocity amplitude measured on the transverse component of station RDM is 3.48 mm/s. Thus, from equation (1), the peak shear strain is 1.32  $\mu$  strain. This value is on the same order as strain values reported to trigger tremor in previous studies (Miyazawa and Mori, 2006; Miyazawa *et al.*, 2008; Rubinstein *et al.*, 2009).

Next, we estimate the maximum shear stress using  $\tau_{\max} = 2\mu(\frac{\partial u_x}{\partial y})$ . We estimate the shear modulus,  $\mu$ , as 27.9 GPa from the shear-wave velocity given in the SCEC CVM-H6.2 (Suess and Shaw, 2003; Plesch *et al.*, 2011). The peak shear stress parallel to fault strike is approximately 35 kPa. To constrain the peak shear stress necessary to trigger tremor, we also estimated the peak shear stress induced by the 2010  $M_w$  7.4 and the  $M_w$  8.8 Maule earthquake, which has next highest peak velocity compared to the Denali earthquake but did not trigger tremor. We estimated the peak shear stress as 17 kPa. Thus, if a purely amplitude-based threshold is necessary to trigger tremor along the SJF, the threshold is likely to be between 17 and 35 kPa.

The threshold we obtained is at the high end of most values previously reported for triggered tremor along subduction zones. Most studies report the dynamic stress threshold sufficient to trigger tremor using peak ground velocity (PGV) rather than strain or stress (e.g., Rubinstein *et al.*, 2007, 2009; Chao, Peng, Fabian, *et al.*, 2012; Chao, Peng, Wu, *et al.*, 2012). In Cascadia on Vancouver Island, the peak stresses reported to trigger tremor were 43 kPa for Love wave and 12 kPa for Rayleigh wave, based on the peak velocity amplitude measures (Rubinstein *et al.*, 2007). In Taiwan under the central range detachment, Peng and Chao (2008) first reported that Love waves from the 2001  $M_w$  7.8 Kunlun earthquake triggered tremor with an estimated shear stress of  $\sim 60$  kPa. However, more recent observations of tremor triggered during several teleseismic events suggest the minimum shear stress required may be as low as 7–8 kPa (Chao, Peng, Wu, *et al.*, 2012). Miyazawa *et al.* (2008) reported that the 2008  $M_w$  7.9 Wenchuan earthquake triggered NVT in Shihoku, Japan, with shear-stress change on the order of 30 kPa, and normal stress change of 40 kPa. These stress changes are estimated at tremor-source depth, around 30 km.

According to Hill (2012b; their Appendix), the shear strain decreases by, at most, 12% from surface to 15 km depth, for a 20 s period Love wave. Even with such decay with depth, the stress changes Chao, Peng, Wu, *et al.* (2012) report for Taiwan would still be lower than our estimate of stress changes along the SJF.

We also compare our estimated triggering threshold to previous studies of triggered tremor along the SAF, which may be a better analog to the SJF than subduction-zone settings. During the Denali earthquake, Peng *et al.* (2008) examined triggered tremor on the SAF and estimated peak-shear-stress changes of approximately 10–20 kPa at the tremor-source depth. This shear-stress change is smaller than what we estimate here for the SJF (17–35 kPa). In a more extensive study, Peng *et al.* (2009) examined 31 teleseismic earthquakes and found 10 examples of triggered tremor; they estimate the threshold required to trigger tremor along the SAF near Cholame is  $\sim 2$ –3 kPa. Hill *et al.* (2013) report that the 11 March 2011  $M_w$  9.0 Tohoku earthquake triggered tremor along the Parkfield section of SAF with an estimated peak dynamic Coulomb stress of 0.7–10 kPa. Thomas *et al.* (2009) reported modulation of tremor amplitudes by tidal stresses on the order of 0.1 kPa. Chao, Peng, Fabian, *et al.* (2012) determined the strain-triggering thresholds of tremor for both northern and southern California. To appropriately compare the triggering thresholds, it is necessary to report the thresholds in consistent method and unit (e.g., stress). We converted the PGV thresholds reported in their study (Fig. 5; Chao, Peng, Fabian, *et al.*, 2012) to stress using the method described in the *Surface-Wave Stress and Strain Estimates* section. The peak stress thresholds are approximately 27, 1.4, and 34 kPa for northern, central, and southern California, respectively. The threshold we obtain here for the SJF (17–35 kPa) is in good agreement with the 34 kPa reported in their study for the same section of the SJF. Thus, the SJF appears to require a higher stress threshold to trigger tremor than the well-studied SAF in central California. The higher stress threshold combined with the infrequent occurrence of triggering may suggest that material properties along the SJF are not as favorable for tremor production as in other locations. More specifically, in contrast to the relatively weak Parkfield–Cholame section of SAF (e.g., Carpenter *et al.*, 2011), the strength of the SJF fault may be greater. This is also suggested by the fact that there is minimal direct evidence for aseismic creep or slow slip in this region.

It is worth noting that we did not observe a clear modulation of the tremor amplitude as the amplitude of Denali surface waves changed. This is in contrast to triggered tremor observed at Parkfield or along subduction zones, where the tremor amplitudes appear to be modulated by small stress perturbations (e.g., tides, Rubinstein *et al.*, 2008; Thomas *et al.*, 2009; teleseismic waves, Chao, Peng, Fabian, *et al.*, 2012; Chao, Peng, Wu, *et al.*, 2012). This may suggest that the SJF has a less well-developed fault core (e.g., higher coefficient of friction), lower pore fluid pressure (e.g., higher effective normal stress), or is not as critically stressed.

### 2009 $M_w$ 6.9 Gulf of California Earthquake

Although the amplitude of induced shear strain during surface waves may play an important role in triggering tremor, whether this factor solely controls the triggering of tremor remains an open question. In the case of earthquake triggering, [Gomberg and Johnson \(2005\)](#) suggest that strain amplitudes that exceed a threshold may be a critical, but not the only, condition necessary to trigger earthquakes remotely. However, they suggest that triggering is not a function of the dominant period of the imposed stress. We do not exclude the possibility that dominant period may affect triggering of tremor. In an attempt to validate whether the dominant period is a factor for triggering tremor, we examine a regional earthquake that induces peak strains larger than those observed during the 2002 Denali earthquake. The 2009  $M_w$  6.9 Gulf of California earthquake occurred significantly closer to the Anza array (583 km) than the 44 teleseismic events that we evaluated in the previous sections. The peak strain observations from the Gulf of California earthquake are 1937 and 1497  $\mu$  strain in the fault-normal and fault-parallel directions, respectively (Table 1; event number 32). These strains, estimated from seismic velocity records, are  $\sim 1.5$  times larger, on average, than those induced by the 2002 Denali earthquake (Table 1). However, the 10.2 s dominant period of this event is significantly shorter than the dominant period during the Denali earthquake and is also the shortest period observed of all the events examined (Fig. 10). Surface waves with short dominant periods decay more rapidly with depth; so, we expected a 30% decrease in amplitude at 15 km depth for a Love wave with a dominant period of 10 s, compared with a 12% decrease for a dominant period of 20 s ([Hill, 2012b](#); their Appendix). However, the estimated strain induced by the 2009 Gulf of California earthquake at the estimated tremor depths is still  $\sim 1.4$  times larger than strain induced by the 2002 Denali earthquake. Although the 2009 Gulf of California earthquake induced larger strains, it does not trigger any observable tremor in the Anza region. If exceeding a given strain threshold were the only condition necessary to trigger tremor, then we would have expected to observe tremor during this event.

### Dominant Period Required for Triggering

Among recent tremor studies, the period of the incoming surface wave is also considered a crucial factor in remote triggering of tremor ([Rubinstein et al., 2009](#); [Chao, Peng, Fabian, et al., 2012](#); [Hill, 2012b](#)). [Rubinstein et al. \(2009\)](#) show that tremor-triggering events have predominant periods between 20–100 s along the Cascadia subduction zone. [Chao, Peng, Wu, et al. \(2012\)](#) suggests that periods above 30 s do not trigger tremor on the detachment fault beneath Taiwan. For low-angle thrust faults in subduction zones, triggered tremor were observed during Rayleigh wave with 10–30 s periods (e.g., 15–30 s for southwest Japan, [Miyazawa et al., 2008](#);  $\sim 20$ –40 s for Cascadia, [Rubinstein et al., 2009](#); 10–30 s for Taiwan, [Chao, Peng, Wu, et al., 2012](#)). Along the SAF at Parkfield, surface waves of 20–30 s period trigger tremor,

although the exact values for each event were not documented ([Peng and Chao, 2008](#)). We selected teleseismic earthquakes with surface waves of a wide range of dominant periods (18.5–103 s; Table 1 and Fig. 10). Only one observed triggered-tremor episode was observed and triggered by Love wave with a period of 23.5 s period; this period falls within the range observed in previous studies. The 2009  $M_w$  6.9 Gulf of California earthquake induced the highest strains, but had the shortest observed surface-wave periods. And, the 2010  $M_w$  7.4, the aftershock of the  $M_w$  8.8 Maule earthquake, induced relatively high strains, but had a relatively long period of surface waves (76 s). Neither of these events triggered tremor in the Anza region. Based on these observations, tremor in the Anza region may respond to dynamic stress change that is dependent not only on exceeding a certain amplitude threshold, but also within a specific period range.

[Ide et al. \(2007\)](#), [Ito et al. \(2007\)](#), and [Shelly et al. \(2011\)](#) proposed the physical mechanism for tremor that is commonly accepted in the seismology community: tremor occurs on small stick-slip asperities on a fault that is primarily slipping by aseismic creep. The tremor source is of limited dimension and higher shear stress than the surrounding area. Both the tremor-source dimensions and the increment of shear stress required to nucleate tremor vary in different regions. The dominant period may correspond to the time scale required for an asperity of a given length to develop into a tremor source. However, further observations of tremor triggered by large earthquakes are needed to constrain the stress threshold and range of periods for this region.

### Love-Wave Triggering

We examine whether the tremor episode that occurred during the Denali earthquake was initiated by Love or Rayleigh energy. The horizontal components were rotated to radial and transverse directions to identify the Love- and Rayleigh-wave arrivals. We then plotted the particle motion of the surface waves for several windows around the tremor episode. We show the onset of the tremor closely matches the Love-wave arrival (Fig. 8). And the particle motion plots show energy primarily in the transverse direction at time of the initial tremor onset (Fig. 11). Tremor continues after the Rayleigh-wave arrival, but the peaks in the tremor are not clearly modulated by the larger Rayleigh-wave amplitudes. Therefore, it is most likely that the tremor is triggered primarily by the Love wave.

[Hill \(2012a\)](#) examined how the triggering potential of Love and Rayleigh wave varies with back azimuth, for vertical strike-slip faults. In an ideal case, the Love-wave triggering potential is at a maximum when the back azimuth is parallel or normal to fault strike and minimized at  $45^\circ$  to fault strike ([Hill, 2012a](#)). The Denali earthquake had a back azimuth of  $338^\circ$ , which was approximately  $18^\circ$  from the fault-parallel direction (strike  $320^\circ$ ). If we examine the 2009  $M_w$  6.9 Gulf of California event, a regional earthquake with larger amplitude of surface-wave arrivals, we find that the back azimuth

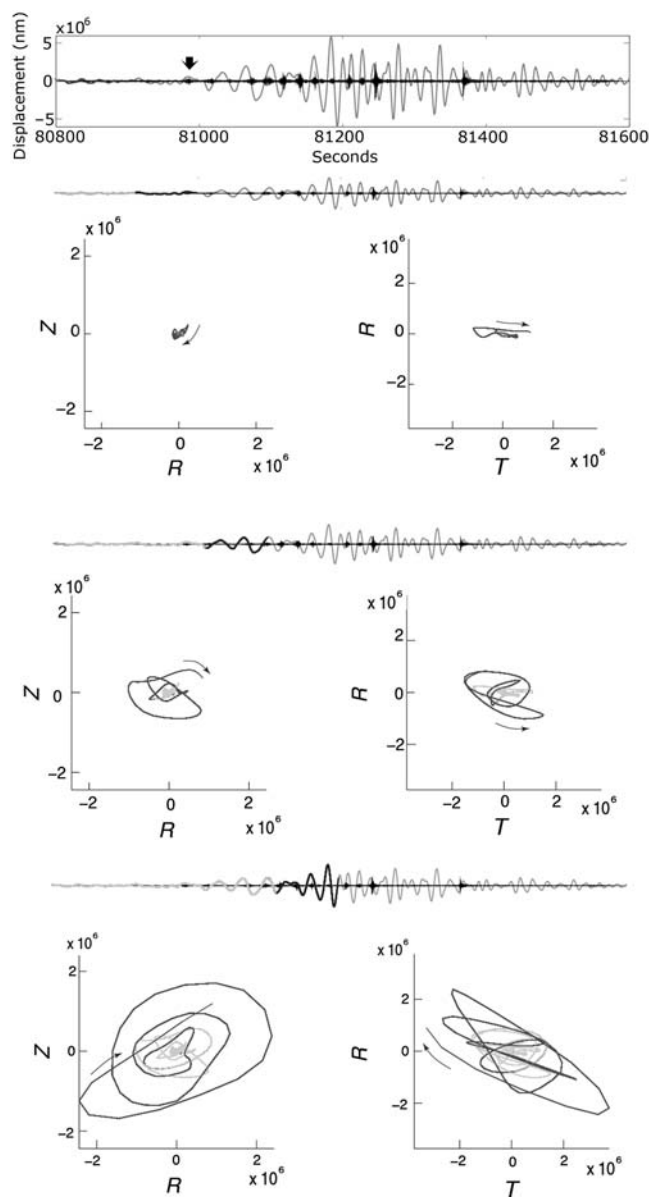


**Figure 11.** Particle-motion plots of the displacement records during different windows of the surface-wave arrivals. Upper plot shows the surface-wave record of Denali earthquake rotated to the transverse direction (gray trace) and the upscaled, filtered trace (black trace). The bold black arrow indicates the start of clear tremor arrivals detected manually and by cross correlation. The lower plots show the particle motion for three consecutive time windows. Gray and black waveform traces are as described above. The heavy black portion of the trace corresponds to the 40 s window used to plot the two particle-motion plots and the light gray trace shows the previous 60 s. The thin black arrows on the particle motion plots indicate the direction of motion at the end of the 40 s window. The two particle motions are (left) in the vertical ( $Z$ ) and radial ( $R$ ) directions (to identify Rayleigh arrivals), and (right) in radial ( $R$ ) and transverse ( $T$ ) directions (to identify Love-wave arrivals).

was also favorably oriented relative to the fault strike. This event had a back azimuth of  $146^\circ$ , approximately  $16^\circ$  from fault parallel. Thus, the back azimuths of these two events were favorable to trigger tremor. Triggered tremor was only

observed during the Denali earthquake, again suggesting amplitude was not the single controlling factor.

## Conclusion and Summary

Over a 10 yr period, between 2001 and 2011, we observed only one episode of tremor triggered by teleseismic arrivals along the SJF near Anza, California. A 5 min long tremor episode comprising 12 tremor pulses occurred during the passage of teleseismic Love waves from the 2002  $M$  7.8 Denali earthquake. The tremor episode was well recorded by 11 surface seismometers. Manually selected templates from the tremor pulses, or LFEs, were found to be highly correlated with each other, suggesting that the tremor originated in a small source region. Although our estimate of tremor depth is not well constrained (5–21 km depth), the triggered tremor or LFEs in Anza appear to be shallower than observed in other regions. Out of all the earthquakes examined, Denali-earthquake surface waves (Love waves) had the second-highest peak shear stress and the second-longest dominant period (22.8 s). This suggests that high peak stress is an important, but not sufficient, condition to trigger tremor and that the dominant period of the surface waves may also play a role. Triggered tremor appears to occur less frequently along SJF compared to other regions that are known to have tremor. And the peak shear stress required to trigger tremor is higher than most other regions where tremor are reported. This is likely related to the specific frictional properties of the SJF fault in this location, which result in only occasional tremor. Alternately, as the overall slip rate along the SJF fault is lower than the SAF, for example, this may result in relatively infrequent triggered tremor.

## Data and Resources

The broadband-velocity seismograms used in this study were collected from Southern California Earthquake Center (SCSN), through the SCEC Seismic Transfer Program (STP). These records can also be obtained from Incorporate Research Institutes of Seismology (IRIS) Data Management Center at [www.iris.edu](http://www.iris.edu) (last accessed January 2013). The borehole velocity seismograms used in this study were obtained from IRIS Data Management Center. The instrument responses for all seismic records were collected from IRIS Data Management Center (SeismicQuery, <http://www.iris.edu/SeismicQuery/> last accessed March 2013). The observed surface-strain records from station Piæon Flat Observatory (PFO) were provided by Institute of Geophysics and Planetary Physics of the University of California, San Diego (IGPP-UCSD). Processed data can be obtained from <http://www.ncedc.org/pbo/strain/processed/lsm> (last accessed February, 2013), or by contacting Duncan Agnew ([dagnew@ucsd.edu](mailto:dagnew@ucsd.edu)). The velocity model used to locate tremor was averaged from the Southern California Earthquake Center Community Velocity Model (SCECVM-H 6.2; [Suess and Shaw, 2003](#); [Plesch et al., 2011](#)). Tremor locations used the Antelope, Boulder Real

Time Technologies (BRIT, 2007), GENeralized LOcation (GENLOC; Pavlis *et al.*, 2004) library, using travel-time interface derived from an averaged Earth velocity model from SCEC CVM-H 6.2. Focal mechanisms of 45 large teleseismic events were obtained from Global Centroid-Moment-Tensor (CMT) database supported by Global CMT Project (<http://www.globalcmt.org/CMTsearch.html>, last accessed March 2013). All other data used in this paper came from published sources.

## Acknowledgments

This work was supported by SCEC 2009 Grant Number 09054 and NSF Grant Number 0943892. We thank Joan Gomberg, David Hill, Hector Gonzalez-Huizar, and an anonymous reviewer for their thoughtful and constructive reviews.

## References

- Aguiar, A. C., J. R. Brown, and G. C. Beroza (2009). Non-volcanic tremor near the Calaveras fault triggered by  $M_w \sim 8$  teleseisms, *Eos Trans. AGU* **90**, no. 54 (Fall Meet. Suppl.), Abstract T23E-06.
- Bailey, I. W., Y. Ben-Zion, T. W. Becker, and M. Holschneider (2010). Quantifying Focal Mechanism Heterogeneity for Fault Zones in Central and Southern California, *Geophys. J. Int.*, doi: [10.1111/j.1365-246X.2010.04745.x](https://doi.org/10.1111/j.1365-246X.2010.04745.x).
- Brown, J. R. (2010). A catalog of low frequency earthquake activity from triggered tremor on the San Jacinto fault, in *SCEC Annual Meeting*, Palm Springs, California, 11–15 September 2010, Abstract 198.
- Brown, K. M., M. D. Tryon, H. R. DeShon, L. M. Dorman, and S. Y. Schwartz (2005). Correlated transient fluid pulsing and seismic tremor in the Costa Rica subduction zone, *Earth Planet Sci. Lett.* **238**, nos. 1–2, 189–203.
- Carpenter, B. M., C. Marone, and D. M. Saffer (2011). Weakness of the San Andreas fault revealed by samples from the active fault zone, *Nature Geosci.* **4**, no. 4, 251–254.
- Chao, K., Z. Peng, A. Fabian, and L. Ojha (2012). Comparisons of triggered tremor in California, *Bull. Seismol. Soc. Am.* **102**, no. 2, 900–908.
- Chao, K., Z. Peng, C. Wu, C.-C. Tang, and C.-H. Lin (2012). Remote triggering of non-volcanic tremor around Taiwan, *Geophys. J. Int.* **188**, no. 1, 301–324.
- Gomberg, J., and D. Agnew (1996). The accuracy of seismic estimates of dynamic strains: An evaluation using strainmeter and seismometer data from Piñon Flat observatory, California, *Bull. Seismol. Soc. Am.* **86**, no. 1A, 212–220.
- Gomberg, J., and P. Johnson (2005). Seismology: Dynamic triggering of earthquakes, *Nature* **437**, no. 7060, 830–830.
- Gomberg, J., P. Bodin, and P. A. Reasenberg (2003). Observing earthquakes triggered in the near field by dynamic deformations, *Bull. Seismol. Soc. Am.* **93**, 118–138.
- Gomberg, J., J. L. Rubinstein, Z. Peng, K. C. Creager, J. E. Vidale, and P. Bodin (2008). Widespread triggering of nonvolcanic tremor in California, *Science* **319**, 173.
- Gonzalez-Huizar, H., A. A. Velasco, Z. Peng, and R. Castro (2012). Remote triggered seismicity caused by the 2011,  $M$  9.0 Tohoku-Oki, Japan earthquake, *Geophys. Res. Lett.* **39**, doi: [10.1029/2012GL051015](https://doi.org/10.1029/2012GL051015).
- Hartse, H. E., M. C. Fehler, R. C. Aster, J. S. Scott, and F. L. Vernon (1994). Small-scale stress heterogeneity in the Anza seismic gap, southern California, *J. Geophys. Res.* **99**, no. B4, 6801–6818.
- Heaton, T. H., and D. V. Helmberger (1977). A study of the strong ground motion of the Borrego Mountain, California earthquake, *Bull. Seismol. Soc. Am.* **67**, no. 2, 315–330.
- Hill, D. P. (2012a). Dynamic stresses, Coulomb failure, and remote triggering—Corrected, *Bull. Seismol. Soc. Am.* **102**, no. 6, 2313–2336.
- Hill, D. P. (2012b). Surface-wave potential for triggering tectonic (non-volcanic) tremor corrected, *Bull. Seismol. Soc. Am.* **102**, no. 6, 2337–2355.
- Hill, D. P., Z. Peng, D. R. Shelly, and C. Aiken (2013). S-wave triggering of tremor beneath the Parkfield, CA, section of the San Andreas fault by the 2011 Tohoku Japan earthquake: Observations and theory, *Bull. Seismol. Soc. Am.* **103**, no. 2B, 1541–1550.
- Hill, D. P., P. A. Reasenberg, A. Michael, W. J. Arabaz, G. Beroza, D. Brumbaugh, J. N. Brune, R. Castro, S. Davis, D. dePolo, W. L. Ellsworth, J. Gomberg, S. Harmsen, L. House, S. M. Jackson, M. J. S. Johnston, L. Jones, R. Keller, S. Malone, L. Munguia, S. Nava, J. C. Pechmann, A. Sanford, R. W. Simpson, R. B. Smith, M. Stark, M. Stickney, A. Vidal, S. Walter, V. Wong, and J. Zollweg (1993). Seismicity remotely triggered by the magnitude 7.3 Landers, California earthquake, *Science* **260**, 1617–1622.
- Ide, S., D. R. Shelly, and G. C. Beroza (2007). Mechanism of deep low frequency earthquakes : Further evidence that deep non-volcanic tremor is generated by shear slip on the plate interface, *Geophys. Res. Lett.* **34**, L03308, doi: [10.1029/2006GL028890](https://doi.org/10.1029/2006GL028890).
- Ito, Y., K. Obara, K. Shiomi, S. Sekine, and H. Hirose (2007). Slow earthquakes coincident with episodic tremors and slow slip events, *Science* **315**, 503–506.
- Kanamori, H. (1980). The state of stress in the Earth's lithosphere, in *Physics of the Earth's Interior*, A. M. Dziewonski and E. Boschi (Editors), Soc. Italiana di Fisica, North-Holland Pub. Co., Amsterdam, 531–554.
- Kendrick, K. J., D. M. Morton, S. G. Wells, and R. W. Simpson (2002). Spatial and temporal deformation along the northern San Jacinto fault, southern California: Implications for slip rates, *Bull. Seismol. Soc. Am.* **92**, no. 7, 2782–2802.
- Louie, J.N., C.R. Allen, D.C. Johnson, P.C. Haase, and S.N. Cohn (1985). Fault slip in southern California, *Bull. Seis. Soc. Am.* **75**, 811–833.
- Mikumo, T., and K. Aki (1964). Determination of local phase velocity by intercomparison of seismograms from strain and pendulum instruments, *J. Geophys. Res.* **69**, no. 4, 721–731.
- Miyazawa, M., and E. E. Brodsky (2008). Deep low-frequency tremor that correlates with passing surface waves, *J. Geophys. Res.* **113**, no. B1, B01307, doi: [10.1029/2006JB004890](https://doi.org/10.1029/2006JB004890).
- Miyazawa, M., and J. Mori (2005). Detection of triggered deep low-frequency events from the 2003 Tokachi-oki earthquake, *Geophys. Res. Lett.* **32**, no. 10, L10307, doi: [10.1029/2005GL022539](https://doi.org/10.1029/2005GL022539).
- Miyazawa, M., and J. Mori (2006). Evidence suggesting fluid flow beneath Japan due to periodic seismic triggering from the 2004 Sumatra–Andaman earthquake, *Geophys. Res. Lett.* **33**, no. 5, L05303.
- Miyazawa, M., E. E. Brodsky, and J. Mori (2008). Learning from dynamic triggering of low-frequency tremor in subduction zones, *Earth Planets Space* **60**, e17–e20.
- Nadeau, R. M., and D. Dolenc (2005). Nonvolcanic tremors deep beneath the San Andreas fault, *Science* **307**, no. 5708, 389.
- Obara, K. (2002). Nonvolcanic deep tremor associated with subduction in southwest Japan, *Science* **296**, 1679–1681.
- Obara, K., H. Hirose, F. Yamamizu, and K. Kasahara (2004). Episodic slow slip events accompanied by non-volcanic tremors in southwest Japan subduction zone, *Geophys. Res. Lett.* **31**, no. 23, L23602, doi: [10.1029/2004GL020848](https://doi.org/10.1029/2004GL020848).
- Pavlis, G. L., F. Vernon, D. Harvey, and D. Quinlan (2004). The generalized earthquake-location (GENLOC) package: An earthquake-location library, *Comput. Geosci.* **30**, nos. 9–10, 1079–1091.
- Peng, Z., and K. Chao (2008). Non-volcanic tremor beneath the Central Range in Taiwan triggered by the 2001  $M_w$  7.8 Kunlun earthquake, *Geophys. J. Int.* **175**, no. 2, 825–829.
- Peng, Z., J. E. Vidale, K. C. Creager, J. L. Rubinstein, J. Gomberg, and P. Bodin (2008). Strong tremor near Parkfield, CA, excited by the 2002 Denali fault earthquake, *Geophys. Res. Lett.* **35**, L23305, doi: [10.1029/2008GL036080](https://doi.org/10.1029/2008GL036080).
- Peng, Z., J. E. Vidale, A. G. Wech, R. M. Nadeau, and K. C. Creager (2009). Remote triggering of tremor along the San Andreas fault in

- central California, *J. Geophys. Res.* **114**, B00A06, doi: [10.1029/2008JB006049](https://doi.org/10.1029/2008JB006049).
- Petersen, M. D., and S. G. Wesnousky (1994). Fault slip rates and earthquake histories for active faults in southern California, *Bull. Seismol. Soc. Am.* **84**, no. 5, 1608–1649.
- Plesch, A., J. H. Shaw, C. Benson, W. A. Bryant, S. Carena, M. Cooke, J. Dolan, G. Fuis, E. Gath, L. Grant, E. Hauksson, T. Jordan, M. Kamerling, M. Legg, S. Lindvall, H. Magistrale, C. Nicholson, N. Niemi, M. Oskin, S. Perry, G. Planansky, T. Rockwell, P. Shearer, C. Sorlien, M. P. Suss, J. Suppe, J. Treiman, and R. Yeats (2007). Community fault model (CFM) for southern California, *Bull. Seismol. Soc. Am.* **97**, no. 6, 1793–1802.
- Plesch, A., C. Tape, R. Graves, P. Small, G. Ely, and J. H. Shaw (2011). Updates for the CVM-H including new representations of the offshore Santa Maria and San Bernardino basin and a new Moho surface, *SCEC Annual Meeting*, Proceedings and abstracts, Vol. 21, Palm Springs, Florida.
- Prejean, S. G., D. P. Hill, E. E. Brodsky, S. E. Hough, M. J. S. Johnston, S. D. Malone, D. H. Oppenheimer, A. M. Pitt, and K. B. Richards-Dinger (2004). Remotely triggered seismicity on the United States West Coast following the  $M_w$  7.9 Denali fault earthquake, *Bull. Seismol. Soc. Am.* **94**, no. 6B, S348–S359.
- Rockwell, T., C. Loughman, and P. Merifield (1990). Late quaternary rate of slip along the San Jacinto fault zone near Anza, southern California, *J. Geophys. Res.* **95**, 8593–8606.
- Rogers, G., and H. Dragert (2003). Episodic tremor and slip on the Cascadia subduction zone: The chatter of silent slip, *Science* **300**, no. 5627, 1942–1943.
- Rubinstein, J. L., J. Gomberg, J. E. Vidale, A. G. Wech, H. Kao, K. C. Creager, and G. Rogers (2009). Seismic wave triggering of nonvolcanic tremor, episodic tremor and slip, and earthquakes on Vancouver Island, *J. Geophys. Res.* **114**, no. B2, B00A01(22), doi: [10.1029/2008JB005875](https://doi.org/10.1029/2008JB005875).
- Rubinstein, J. L., M. L. Rocca, J. E. Vidale, K. C. Creager, and A. G. Wech (2008). Tidal modulation of nonvolcanic tremor, *Science* **319**, 186.
- Rubinstein, J. L., D. R. Shelly, and W. L. Ellsworth (2010). Non-volcanic tremor: A window into the roots of fault zones, in *New Frontiers in Integrated Solid Earth Sciences*, S. Cloetingh and J. Negendank (Editors), Springer, Netherlands, 287–314.
- Rubinstein, J. L., J. E. Vidale, J. Gomberg, P. Bodin, K. C. Creager, and S. D. Malone (2007). Non-volcanic tremor driven by large transient shear stresses, *Nature* **448**, 579–582.
- Sanders, C. O. (1990). Earthquake depths and the relation to strain accumulation and stress near strike-slip faults in southern California, *J. Geophys. Res.* **95**, 4751–4762.
- Sanders, C. O., and H. Kanamori (1984). A seismotectonic analysis of the Anza seismic gap, San Jacinto fault zone, southern California, *J. Geophys. Res.* **89**, 5873–5890.
- Sanders, C. O., and H. Magistrale (1997). Segmentation of the northern San Jacinto fault zone, southern California, *J. Geophys. Res.* **102**, no. B12, 27453–27467.
- Schwartz, S. Y., and J. M. Rokosky (2007). Slow slip events and seismic tremor at circum-Pacific subduction zones, *Rev. Geophys.* **45**, RG3004, doi: [10.1029/2006RG000208](https://doi.org/10.1029/2006RG000208).
- Sharp, R. V. (1967). San Jacinto fault zone in the Peninsular ranges of southern California, *Geol. Soc. Am. Bull.* **78**, 705–730.
- Shelly, D. R., and J. L. Hardebeck (2010). Precise tremor source locations and amplitude variations along the lower-crustal central San Andreas fault, *Geophys. Res. Lett.* **37**, no. 14, L14301.
- Shelly, D. R., G. C. Beroza, S. Ide, and S. Nakamura (2006). Low-frequency earthquakes in Shikku, Japan, and their relationship to episodic tremor and slip, *Nature* **442**, 188–191.
- Shelly, D. R., W. L. Ellsworth, T. Ryberg, C. Haberland, G. S. Fuis, J. Murphy, R. M. Nadeau, and R. Burgmann (2009). Precise location of San Andreas fault tremors near Cholame, California using seismometer clusters: Slip on the deep extension of the fault? *Geophys. Res. Lett.* **36**, L01303.
- Shelly, D. R., Z. Peng, D. P. Hill, and C. Aiken (2011). Triggered creep as a possible mechanism for delayed dynamic triggering of tremor and earthquakes, *Nature Geosci.* **4**, no. 6, 384–388.
- Sieh, K. (1986). Slip rate across the San Andreas fault and prehistoric earthquakes at Indio, *Eos Trans. AGU* **67**, 1200.
- Steidl, J., M. Gladwin, R. Gwyther, and F. Vernon (2000). Fault processes on the Anza section of the San Jacinto fault, *The Anza Broadband Seismic 24-bit Real-Time Telemetry Network Year 2000 Proposal*, UCSD, San Diego, California, 1–5.
- Suess, M. P., and J. H. Shaw (2003). P wave seismic velocity structure derived from sonic logs and industry reflection data in the Los Angeles basin, California, *J. Geophys. Res.* **108**, no. B3, 2170.
- Sykes, L. R., and S. P. Nishenko (1984). Probabilities of occurrence of large plate rupturing earthquakes for the San Andreas, San Jacinto, and Imperial faults, California, 1983–2003, *J. Geophys. Res.* **89**, no. B7, 5905–5927.
- Thatcher, W., J. A. Hileman, and T. C. Hanks (1975). Seismic slip distribution along the San Jacinto fault zone, southern California, and its implications, *Bull. Seismol. Soc. Am.* **86**, no. 8, 1140–1146.
- Thomas, M. A., R. M. Nadeau, and R. Burgmann (2009). Tremor-tide correlations and near-lithostatic pore pressure on the deep San Andreas fault, *Nature* **462**, 1048–1051.
- Vanboskirk, E.J., M.H. Gottlieb, K.M. Hodgkinson, D. Mencin, W. Johnson, C. Pyatt, D.B. Henderson, O. Fox, W.W. Gallaher, M.E. Jackson, and the PBO BSM Group (2011). 2011 creep event observations in borehole strainmeter instrumentation along the San Andreas and San Jacinto faults (abstract T13A-2348), *AGU*, presented at 2011 Fall Meeting, San Francisco, California, 5–9 December, T13A-2348.
- Wdowinski, S. (2009). Deep Creep as a cause for the excess seismicity along the San Jacinto fault, *Nat. Geosci.* **2**, 882–885.

University of California, Riverside  
Department of Earth Sciences, R1345  
900 University Ave.  
Riverside, California 92507  
(T.-H.W., D.D.O.)

United States Geological Survey, Pasadena  
525 and 535 S. Wilson Ave.  
Pasadena, California 91106-3212  
(E.S.C.)

Geophysics and Planetary Physics (IGPP)  
IGPP 0225  
University of California  
9500 Gilman Dr  
La Jolla, California 92093-0225  
(D.A.)